Dyes and Pigments 204 (2022) 110467

Contents lists available at ScienceDirect

Dyes and Pigments

journal homepage: www.elsevier.com/locate/dyepig

Tetra-Carbazole based electroactive donor-acceptor dyes: Effect of the phenyl bridging unit on the electrochromic performance

Ceylan Doyranlı [a], Sinem Altınısık [b], Mücahit Özdemir [c], Sermet Koyuncu [b,d,*]

[a] Department of Chemistry, Faculty of Arts and Sciences, Yıldız Technical University, 34220, Istanbul, Turkey
[b] Department of Chemical Engineering, Faculty of Engineering, Canakkale Onsekiz Mart University, 17100, Canakkale, Turkey
[c] Department of Chemistry, Marmara University, 34722, Istanbul, Turkey
[d] Department of Energy Resources and Management, Çanakkale Onsekiz Mart University, 17020, Çanakkale, Turkey

ARTICLE INFO

Keywords:
Donor-acceptor dyes
Carbazole
Quinoxaline
Electrochromic materials

ABSTRACT

In this study, a new Donor-Acceptor-Donor (D-A-D) electroactive molecules (HCQM1 and HCQM2) containing 9H-carbazole and 9-phenyl-9H-carbazole as donor along with quinoxaline (HQ) as acceptor were synthesized and then coated on Indium Tin Oxide/Glass (ITO/Glass) surface by the electrochemical oxidation process. The HOMO-LUMO band gap values obtained by electrochemical oxidation and reduction onsets were calculated as 2.64 and 2.68 eV, respectively. On the other hand, UV–Vis absorption measurements showed that the charge transfer band of HCQM1 was detected at 500 nm with 50 nm red shift upon compared with the HCQM2. According to AFM results, it is seen that the roughness of the poly(HCQM2) film is higher than the poly(HCQM1) film. Finally, the polymer film of HCQM2 showed multi-electrochromic color change (yellow, green, and dark blue) upon the oxidation process. When the electrochromic performance of the HCQM1 and HCQM2 polymer films was compared, it was discovered that the HCQM2 with phenylene spacer unit has better stability and a higher percentage transmittance change (ΔT%) between neutral and oxidized states.

1. Introduction

Electrochromism is defined as the ability of such materials to change their color or optical properties through redox reactions when subjected to a small external voltage or current [1]. Electrochromic materials are of great interest in academia and industry due to their changing color when exposed to small electrochemical signals [2]. Multilayer transparent conductive architectures consisting of ion conductive electrolyte layers, ion storage layers, and electrochromic active layers are used in the production of electrochromic devices [3–5]. Smart windows, the main application of electrochromic devices, regulate the quantity of visible light and solar radiation entering buildings while also providing energy efficiency by having varying permeability levels [6]. In addition, electrochromic devices are used in combination with other important technologies [7], including wearables [5,8,9], thermal control [10,11], energy storage [12,13], energy harvesting, and sensing technologies [4,14]. Among the electrochromic materials, inorganic metal oxides, organic dyes, and conjugated polymers stand out [15]. Polymeric functional materials with conjugated structures have been developed for optoelectronic applications in recent years [16]. Conjugated polymers are interesting for use in electrochromic devices because of their controllable HOMO-LUMO band gap, low response time, contrast capability, and easily processing when compared to inorganic materials [17,18]. In conjugated polymers, the donor-acceptor strategy is applied to arrange the bandgap and also neutral state color for the polymeric materials [19]. Furthermore, the bandgap of conjugated polymers can be changed by interacting with different donor and acceptor units [20,21].

Carbazole is an aromatic, heterocyclic organic compound that can form a semi-conductive polymer film by oxidation process [22,23]. Conjugated polymer films formed with carbazole derivatives can be used in the components of sensors [24,25], batteries [26,27], organic electroluminescence materials, and electrochromic devices [28,29] owing to their electron donor property, high photoconductivity. It is possible to modify the properties of carbazole-based semi-conductive polymers by adding functional groups with specific qualities to their structure. N-position functionalization of carbazole derivatives with various substituents can be performed to improve polymer solubility and usability [30]. Researchers are interested in quinoxaline, an electron-withdrawing semiconductor material, for usage as an acceptor

* Corresponding author. Department of Chemical Engineering, Faculty of Engineering, Canakkale Onsekiz Mart University, 17100, Canakkale, Turkey.
E-mail address: skoyuncu@comu.edu.tr (S. Koyuncu).

https://doi.org/10.1016/j.dyepig.2022.110467
Received 3 February 2022; Received in revised form 5 May 2022; Accepted 29 May 2022
Available online 3 June 2022

bridge in low bandgap polymer semiconductors. Due to the presence of two sp2-hybridized nitrogen atoms (aromatic C=N), quinoxaline bridges have a high electron affinity and strong electron-accepting characteristics [31,32].

In this study, two new Donor-Acceptor-Donor (D-A-D) compounds (HCQM1 and HCQM2) were synthesized to investigate the spacer unit effect between donor and acceptor moieties on electrochemical, optical, as well as electrochromic properties (Fig. 1). The charge distribution change between the donor and acceptor moieties of HCQM1 and HCQM2 was also supported by theoretical DFT calculations. According to AFM images, the more porous thin film can be obtained from the HCQM2 by electrochemical polymerization process due to its 3D molecular structure when compared to HCQM1. Furthermore, the electrochromic performance of poly(HCQM2) is better than poly(HCQM1) in terms of contrast ratio (%ΔT) response time and also switching stability.

2. Experimental

2.1. Materials

All initial compounds and other chemicals were obtained from Sigma-Aldrich and Merck as commercial suppliers. 3,3'-(5,8-dibromoquinoxaline-2,3-diyl)bis(9-hexyl-9H-carbazole (HCQ) was synthesized in accordance with the previously reported procedures [33,34]. The D−A compounds HCQM1 and HCQM2 were prepared via Suzuki [35] and Ullman Coupling Reaction [36,37], respectively. The synthetic pathway for HCQM1 and HCQM2 as electroactive monomers was presented in Scheme 1. Structural characterization of electroactive moieties was carried out by elemental analysis, FT-IR, ^{1}H NMR, and ^{13}C NMR techniques (see supporting information Figs. S1–S5).

2.2. Synthesis of 3,3'-(5,8-di(9H-carbazol-9-yl)quinoxaline-2,3-diyl)bis (9-hexyl-9H-carbazole) [HCQM1]

HCQ (0.5 g, 0.63 mmol), carbazole (0.23 g, 1.39 mmol), Cu powder (0.08 g, 1.25 mmol), 18-crown-6 (0.16 g, 0.6 mmol), K_2CO_3 (0.52 g, 3 mmol), and nitrobenzene (20 ml) were added to a round-bottom flask and vigorously stirred at 210 °C under argon. After 24 h the reaction solution cooled to room temperature and poured into 250 ml of water and the crude product was purified by column chromatography [silica gel, $CHCl_3$: Hexane (1:1)] to afford pure compound as a yellow solid.

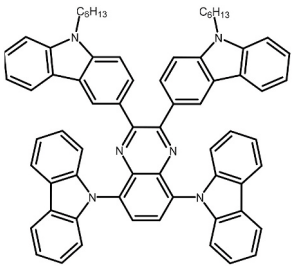

Yield: 372 mg (62%), mp: 112 °C; Anal. Calc. for [$C_{68}H_{58}N_6$] (Mw: 959.25 g/mol): C, 85.14; H, 6.09; N, 8.76%, found: C, 85.15; H, 6.06; N, 8.71%. FT-IR (ATR): ν_{max}, cm^{-1} 3047 (Aromatic C–H), 2920-2851 (Aliphatic C–H), 1625 (N–H) 1597 (Aromatic C=C). ^{1}H NMR ($CDCl_3$ 400 MHz): δ ppm, 8.27 (d, $J = 7.5$ Hz, 4H, H_d); 8.20 (s, 2H, H_l); 8.09 (s, 2H, H_k); 7.71 (d, $J = 7.3$ Hz, 2H, H_h); 7.55–7.29 (m, 14H, H_j, H_e, H_h, H_c, H_g, H_i, H_f); 7.18 (t, $J = 7.4$ Hz, 4H, H_b); 6.94 (d, $J = 8.6$ Hz, 4H, H_a); 4.12 (t, $J = 7.3$ Hz, 4H, -N–CH_2–); 1.72–1.20 (m, 16H, –$(CH_2)_4$–); 0.82–0.74 (m, 6H, –CH_3). ^{13}C NMR ($CDCl_3$, 400 MHz): δ ppm, 153.27; 141.72; 140.64; 140.30; 136.92; 134.05; 128.73; 127.37; 126.96; 125.38; 123.66; 122.78; 120.26; 120.03; 119.77; 118.78; 110.75; 108.39; 107.19; 42.67; 31.10; 28.81; 26.46; 22.12; 13.63.

2.3. Synthesis of 3,3'-(5,8-bis(4-(9H-carbazol-9-yl)phenyl)quinoxaline-2,3-diyl)bis(9-hexyl-9H-carbazole) [HCQM2]

HCQ (0.22 g, 0.25 mmol), 9H-Carbazole-9-(4-phenyl) boronic acid pinacol ester (M2) (0.25 g, 0.67 mmol), 5 ml $K_2CO_{3(aq)}$ (2 M) and 15 mL toluene were added in a 50 ml flask and stirred under argon atmosphere for 30 min. After the stirred adding the $Pd(PPh_3)_4$ (5 mol %) as a catalyst and 1 ml tetraethyl ammonium hydroxide the reaction mixture was refluxed at 110 °C for 24 h. The reaction mixture was then cooled and precipitated in 300 mL of ethyl alcohol. Column chromatography [silica gel, $CHCl_3$: Hexane (1:1)] was performed for final purification. The pure pale yellow product was obtained.

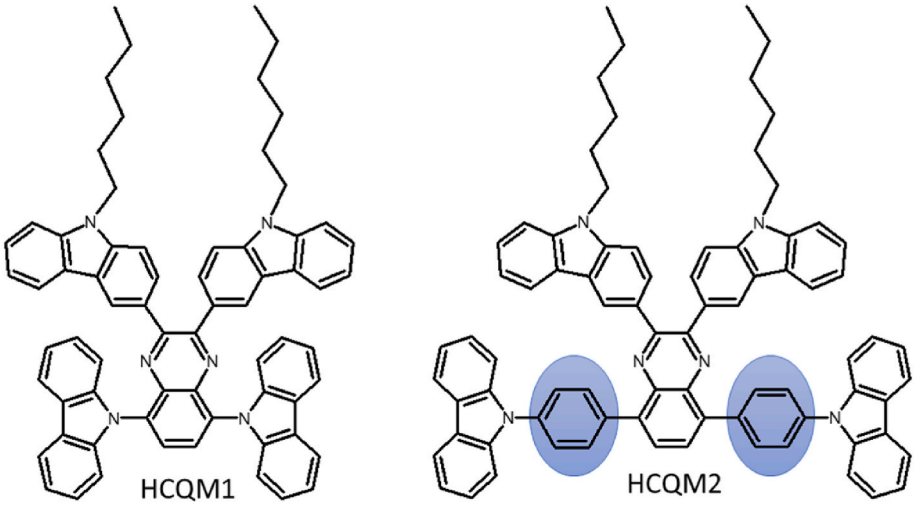

Fig. 1. Chemical structure of HCQM1 and HCQM2.

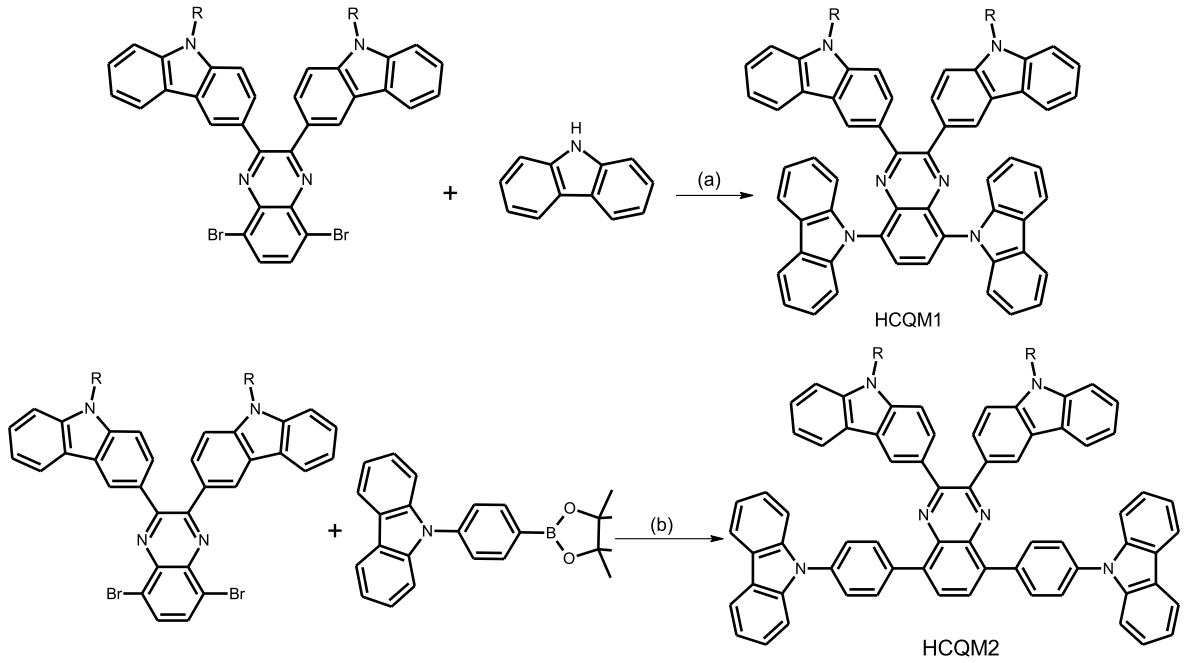

Scheme 1. Synthetic route to HCQM1 (a) and HCQM2 (b) monomers (Reagents and conditions: (a) K_2CO_3, Cu powder, 18-Crown-6, nitrobenzene, 210 °C, 24 h; (b) $Pd(PPh_3)_4$, 3 M K_2CO_3 in water, toluene, 120 °C, 24 h. (R: $-C_6H_{13}$).

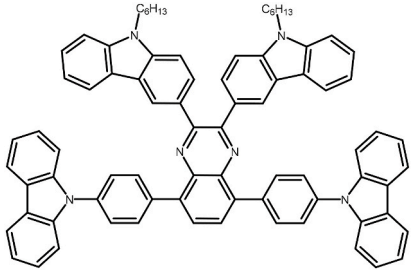

Yield: 186 mg (60%), mp: 124 °C; Anal. Calc. for [$C_{80}H_{66}N_6$] (Mw: 1111.45 g/mol): C, 86.45; H, 5.99; N, 7.56%, found: C, 86.44; H, 5.96; N, 7.51%. FT-IR (ATR): ν_{max}, cm^{-1} 3047 (Aromatic C–H), 2920-2851 (Aliphatic C–H), 1625 (N–H) 1597 (Aromatic C=C). ^1H NMR ($CDCl_3$ 400 MHz): δ ppm, 8.77 (s, 2H, H_l); 8.26 (d, $J = 8.3$ Hz, 4H, H_m); 8.20 (d, $J = 7.8$ Hz, 4H, H_a); 8.05 (s, 2H, H_e); 8.01 (d, $J = 7.7$ Hz, 2H, H_j); 7.87–7.81 (m, 4H, H_n); 7.75 (dd, $J = 8.4$, 1.9 Hz, 2H, H_i); 7.67 (d, $J = 8.3$ Hz 4H, H_d) 7.45–7.21 (m, 16H, H_b, H_c, H_f, H_h, H_k, H_g); 4.24 (t, $J = 7.1$ Hz, 4H, -N–CH_2–); 1.82–1.23 (m, 16H, –$(CH_2)_4$–); 0.81 (t, $J = 7.0$ Hz, 6H, –CH_3). ^{13}C NMR ($CDCl_3$ 400 MHz): δ ppm, 151.88; 140.53; 138.10; 137.18; 136.72; 132.17; 129,67; 128.82; 127.74; 125.99; 125.72; 125.51; 123.12; 122.69; 122.02; 119.97; 119.62; 119.09; 109.72; 108.55; 107.83; 42.84; 31.16; 28.53; 26.56; 22.17; 13.66.

2.4. Electrochemical polymerization

Electrochemical polymerization was carried out by using a DCM solution of 2.0×10^{-3} M HCQM1 and HCQM2 monomers and 0.1 M $TBAPF_6$. Poly(HCQM1) and poly(HCQM2) films were obtained by performing 20 repetitive cycles at potentials between 0 and 1.3 V and 0 and 1.35 V, respectively, at a scanning rate of 100 mV/s. ITO/Glass surface (ITO, 8–12 Ω, active area = 0.8 cm × 2 cm) or Pt disc (0.02 cm^2) were used to obtain the corresponding polymers during the process. In repeated cyclic voltammetry measurement, it was observed that the reversible oxidation waves were formed with the half-wave potential of 0.96 and 1.01V, respectively. An increase in the signals at each repeated scan is revealed by a polymer coating on the ITO/glass used as the working electrode surface (Fig. 2). The polymer films were cleaned with chloroform after the coating procedure to eliminate the electrolyte salt and unreacted monomers.

2.5. Instrumentation

^1H NMR and ^{13}C NMR (Bruker Avance DPX-400) data were registered at 25 °C using $CHCl_3$-d as the solvent and with tetramethylsilane (TMS) as an internal standard. Electrochemical analyzes were performed under an argon atmosphere using a CH Instruments 617D potentiostat/galvanostat system. In this system, Pt disc (0.02 cm^2) as the working electrode (WE), Ag wire (PRE) as a pseudo-reference electrode, Pt wire (CE) as a counter electrode. Electrolyte solution containing 0.1 M $TBAPF_6$ in dichloromethane (DCM) or acetonitrile (ACN) as supporting electrodes was used. Electrochemical studies of HCQM1 and HCQM2 monomers were drop-casted on the Pt disk as the working electrode and then the potential was scanned in the electrolyte solution. Then electrochemical polymerization of both molecules was realized in a dichloromethane solution consisting of $2.0x10^{-3}$ M HCQM1-2 monomer and 0.1 M $TBAPF_6$ at a 100 mV/s scan rate and the polymers were coated on Pt disc or ITO/glass as WE. After all measurements, the electrochemical HOMO-LUMO band gap calculated from the oxidation-reduction onset potentials was calibrated against the ferrocene redox couple (Fig. S6) - Fc/Fc^+ $E^{ox}_{m,a} = 0.38$ V; $E^{ox}_{m,c} = 0.28$ V; $E^{ox}_{1/2} = 0.33$ V (vs Ag wire) in CH_2Cl_2 using the equation $E_{HOMO} = -e(E_{ox\text{-}ons} - E_{Fc}) + (-4.8$ eV) and $E_{LUMO} = -e(E_{red\text{-}ons} - E_{Fc}) + (-4.8$ eV) [38]. Analytic Jena Speedcord S-600 diode-array spectrophotometer was used to measure UV–Vis absorption spectra. The optical band gaps (Eg) of the molecules were calculated from the absorption edges (λ_{onset}) using the equation $Eg = 1241/\lambda_{onset}$ [39]. Photoluminescence (PL) spectra were obtained with the PTI QM1 fluorescent spectrophotometer. Fluorescence Quantum Yields (φ) were calculated according to fluorescein standard molecule.

Spectroelectrochemical measurements were carried out by applying the potential to polymer films on the ITO/glass surface and utilizing absorption spectra. The spectro-electrochemical cell is made up of a quartz cuvette, an Ag wire (PRE), a Pt wire counter electrode (CE), and ITO/glass as a transparent working electrode (WE), and measurements were performed in ACN with 0.1 M $TBAPF_6$ as the supporting electrolyte

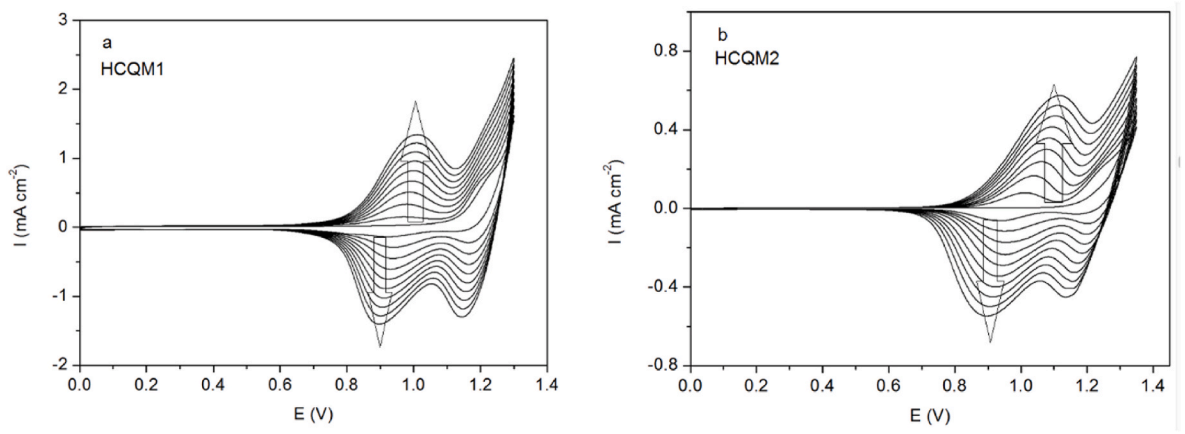

Fig. 2. Repeated potential scans of HCQM1 (a) and HCQM2 (b) monomers in 0.1 M $TBAPF_6$ in DCM, scan rate 100 mV/s.

[40]. The surface morphology of HCQM1-2-based polymer films was examined at ambient conditions using a Nanosurf Naio-AFM. The non-contact mode was used to record topographic and phase images in the system. The measurements were taken by scanning over polymer-coated ITO/glass in a measuring area of 10 × 10 μm^2 under an acoustic chamber.

3. Results and discussion

3.1. Electrochemical properties

The electrochemical behaviors of HCQM1 and HCQM2 monomers and polymers were studied using Cyclic Voltammetry (CV) and Differential Pulse Voltammetry (DPV) (Figs. 3 and 4). Drop cast HCQM1 and HCQM2 electroactive monomer solutions onto the Pt disk working electrode surface yielded cyclic voltammograms in an acetonitrile electrolyte solution. Besides, the polymers were coated on the Pt disk as WE surface via electrochemical potentiodynamic polymerization.

The electrochemical oxidation mechanisms of carbazoles have been described in many studies available in the literature [41,42]. HCQM1 and HCQM2 have an oxidation peaks in the anodic regime at $E^{ox}_{m,a}$ = 1.23 V and $E^{ox}_{m,a}$ = 1.29 V vs. Ag wire, respectively (Table 1). When both HCQM1 and HCQM2 molecules were scanned up to 1.8 V, it was observed that they had multi-step oxidation behavior due to the multiple carbazole groups in their structure (Fig. S7). The donor unit carbazole and the acceptor unit quinoxaline are directly linked in HCQM1, hence the acceptor quinoxaline group directly attracts electrons from the donor carbazole. This interaction is reduced in HCQM2 by the spacer phenylene group between the donor carbazole and quinoxaline. Finally, the spacer effect of the phenylene ring between the carbazole donor and the quinoxaline acceptor could explain the observed oxidation at a higher potential in HCQM2 than in HCQM1. This effect is also clearly shown in theoretical DFT results.

The reduction peak of HCQM1 was found to be at a lower negative potential ($E^{red}_{m,c}$ = -1.59 V) than that of HCQM2 ($E^{red}_{m,c}$ = -1.69 V). Thus, HCQM1 requires less potential for electron addition of the quinoxaline group, which is the common acceptor moiety in both monomers.

Poly(HCQM1) and poly(HCQM2) oxidation peaks formed after the electrochemical polymerization process shifted to a lower potential than the corresponding monomers ($E^{ox}_{m,a}$ = 1.16 V and $E^{ox}_{m,a}$ = 1.13, respectively). However, the reduction potential of the polymers was higher than that of the corresponding monomers. The oxidation and reduction potential peak shift can be due to the increase of conjugation resulting from the carbazole-carbazole coupling. The HOMO-LUMO energy levels were calculated using the oxidation and reduction potential onsets from DPV curves (Fig. 4a–c and Table 1). These results indicate that the HOMO-LUMO band gap is narrowing as a result of the conjugated main chain that occurs after polymerization.

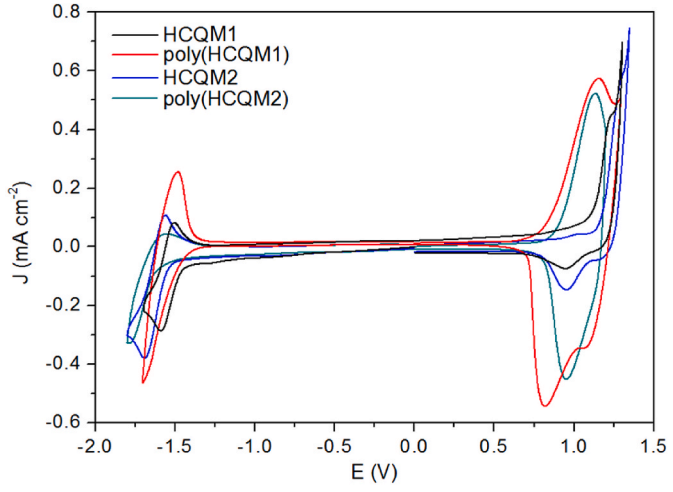

Fig. 3. Cyclic voltammograms of HCQM1/HCQM2 in 0.1 M $TBAPF_6$/ACN electrolyte solution and poly(HCQM1)/poly(HCQM2) in 0.1 M $TBAPF_6$/DCM electrolyte solution at scan rate of 100 mV/s. Ag wire.

3.2. Optical properties

UV–Vis absorption and photoluminescence spectroscopy were used to characterize the optical properties of HCQM1 and HCQM2 electroactive molecules (Fig. 5 and Fig. S8). When the absorption spectra of both molecules were examined, a characteristic peak was observed at 275 and 310 nm attributed to the π-π* and n-π* transitions of the conjugated system, respectively (Fig. 5a). Furthermore, a 35 nm red shift in the charge transfer band of HCQM1 was observed when compared to the absorption spectrum of HCQM2. This could be because the charge localization of the phenylene bridge in the HCQM2 structure is preventing charge transfer from carbazole-donor to quinoxaline-acceptor. A similar effect was observed in the fluorescence spectra of the HCQM1, even though both structures contained the same electroactive moieties. For HCQM1, a yellowish-green band at 536 nm was shifted to 502 nm for HCQM2, corresponding to bright cyan photoluminescence (Fig. S8a). Besides, the Stoke's shifts ($\Delta\nu^{-1}$), fluorescence quantum yields (Φ_f), and molar absorption coefficients (ε_{max}) of HCQM1 and HCQM2 in DCM was shown in Table 2. Apart from this, theoretical UV–Vis absorption spectra and electronic transitions were calculated by TD-DFT calculations. It has been observed that the obtained values are in good agreement with the experimental data (Fig. S9).

The charge transfer band was observed in the thin film absorption

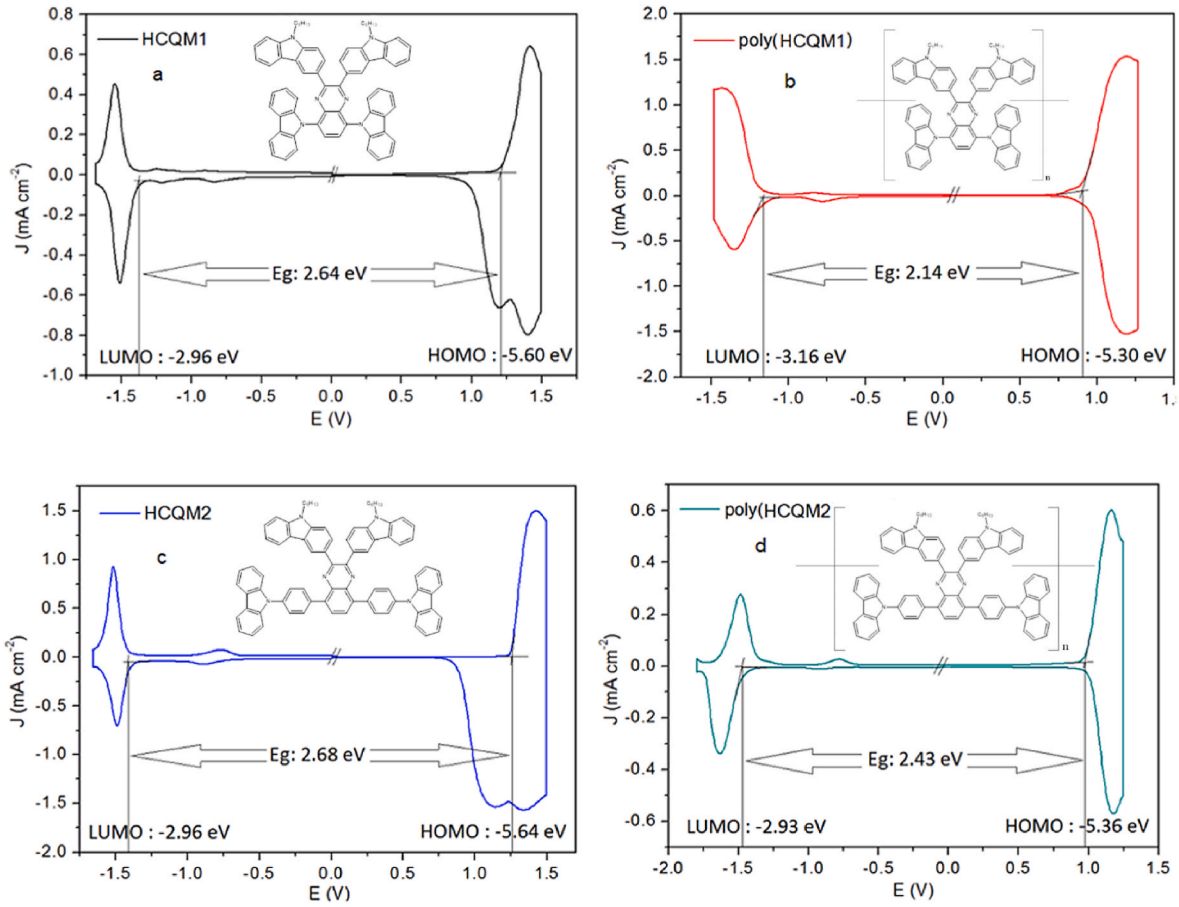

Fig. 4. Redox behavior in DPV of HCQM1 (a), poly(HCQM1) (b), HCQM2 (c) and poly(HCQM2) (d).

Table 1
Optical and Electrochemical values of HCQM1 and HCQM2 monomers and corresponding polymers.

Molecule	Oxidation Peak Potential (V)	Reduction Peak Potential (V)	HOMO (eV)	LUMO (eV)	$E_{gap,\ electrochemical}$ (eV)	$E_{gap,\ optical}$ (eV)
HCQM1	$E^{ox}_{m,a} = 1.23$ $E^{ox}_{m,c} = 0.95$	$E^{red}_{m,a} = -1.51$ $E^{red}_{m,c} = -1.59$	−5.60	−2.96	2.64	2.48
Poly(HCQM1)	$E^{ox}_{p,a} = 1.16$ $E^{ox}_{p,c} = 0.82$	$E^{red}_{p,a} = -1.48$ $E^{red}_{p,c} = -1.68$	−5.30	−3.16	2.14	2.34
HCQM2	$E^{ox}_{m,a} = 1.29$ $E^{ox}_{m,c} = 0.96$	$E^{red}_{m,a} = -1.56$ $E^{red}_{m,c} = -1.69$	−5.64	−2.96	2.68	2.60
Poly(HCQM2)	$E^{ox}_{p,a} = 1.13$ $E^{ox}_{p,c} = 0.95$	$E^{red}_{p,a} = -1.57$ $E^{red}_{p,c} = -1.79$	−5.36	−2.93	2.43	2.48

spectra of the HCQM1 and HCQM2 films obtained by the drop-casting method at approximately 425 and 440 nm for HCQM1 and HCQM2, respectively (Fig. 5b). The emission maxima in the normalized photoluminescence spectra of the films obtained by excitation from the charge transfer band were 535 and 500 nm, respectively (Fig. S8b). Similar absorption and photoluminescence behavior in both solution and thin film demonstrated that the solid-state has a limited intermolecular interaction effect. Table 1 summarizes the optical and electrochemical bandgap data obtained from the UV–vis spectra of HCQM1, HCQM2, and corresponding polymer films. The compatibility of the optical and electrochemical band gap values demonstrated that the neutral state charge transfer from carbazole-donor to quinoxaline-acceptor could be carried out effectively for both molecules. These results obtained from absorption and fluorescence spectra are also supported by theoretically DFT calculations.

3.3. Theoretical calculations

DFT calculations were done with Gaussian 16 [43], and the results were visualized with GaussView 6.0 [44] and IQMol. Geometry optimizations of HCQM1 and HCQM2 were calculated with Becke-3-Lee-Yang-Parr's functional correlation (B3LYP) [45–47] of 6-31G(d,p) level of theory in the DFT method. The Polarizable Continuum Model (PCM) [48,49] in the ground state, as implemented in Gaussian16, was used to explore the solvent impact. The time-dependent DFT approach was used to detect UV–Vis absorption spectra in dichloromethane to see electronic transitions and orbital contributions. Electronic transitions and orbital contributions were calculated using GausSum. Table 3 shows the calculated molecular orbitals (HOMO and LUMO) and energies (E_{HOMO} and E_{LUMO}) for the B3LYP/6-31G (d,p) level monomers. The charges separated from the conjugated carbazole main chain at HOMO

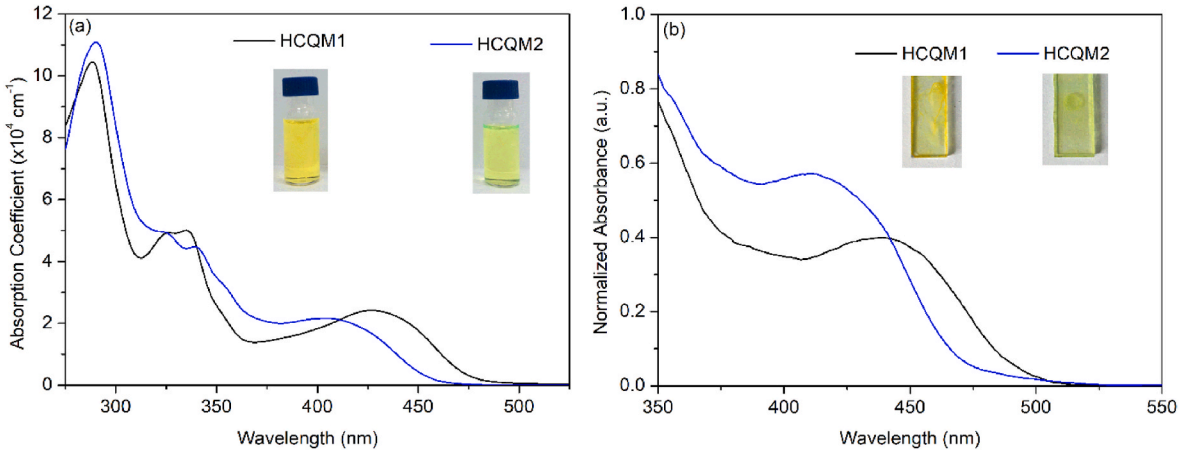

Fig. 5. UV–vis absorption spectra of HCQM1 and HCQM2 monomers in DCM (a) and on thin-film (b).

Table 2
Absorption wavelengths λ_{abs} (nm), emission wavelengths at excitation 485 nm λ_{em} (nm), calculated Stoke's shifts ($\Delta\nu^{-1}$), fluorescence quantum yields (Φ_f), and molar absorption coefficients (ε_{max}) of HCQM1 and HCQM2 in DCM.

Molecule	λ_{abs}/nm	λ^a_{em}/nm	$\Delta\upsilon$/cm^{-1}	φ_f	ε_{max} ($^4_{x10}$)
HCQM1	289,326,335,432	536	4511	0.75	10.45
HCQM2	290,325,341,409	502	4490	0.67	11.09

and pendant carbazole moieties at HOMO-1 for the HCQM1 molecule were transferred to the quinoxaline-based acceptor moieties at LUMO orbitals, according to these findings. On the other hand, the charges separated from the conjugated carbazole and phenyl chain at both HOMO and HOMO-1 orbital of the HCQM2 different from HCQM1 were moved to the quinoxaline-based acceptor part at LUMO orbitals. The HOMO-LUMO band gap calculated by DFT increased from 3.09 eV to 3.21 eV when a phenyl moiety was attached between a carbazole donor and a quinoxaline acceptor. The experimental values showed the same increase in the bandgap. Furthermore, according to 3D optimized geometry, HCQM1 has a more planar structure than HCQM2. Due to the planar structure, the charges could be delocalized for different centers at HOMO and LUMO. This bipolar charge separation at HOMO and LUMO could be advantageous in the use of organic optoelectronic devices as active materials.

3.4. Surface properties

Atomic Force Microscopy (AFM) with tapping-mode was used to characterize the surfaces of electrochemically coated poly(HCQM1) and poly(HCQM2) films. When the roughness values of the polymer films from the height images were compared, it was discovered that the poly (HCQM2) film was more porous than the poly(HCQM1) film (HCQM1). The HCQM1 has a more planar structure in the 3D plane than the HCQM2. Furthermore, the presence of a phenyl ring between the carbazole donor and the quinoxaline acceptor improved the polymer film morphology. Because of their large surface area, porous films are known to have a positive effect on electrochromic performance [50]. As a result, electrolyte ions can easily enter and exit the porous polymer films. The RMS roughness of poly(HCQM1) and poly(HCQM2) was found to be 3.24 nm and 6.42 nm, respectively (Fig. 6).

3.5. Spectroelectrochemical properties

Spectroelectrochemistry was used to characterize radical species formation as well as color change detection in polymer films prepared electrochemically on ITO/glass surfaces. Poly(HCQM1) and poly

Table 3
Calculated molecular orbitals (HOMO and LUMO) energies (E_{HOMO} and E_{LUMO}) for the HCQM1 and HCQM2 monomers.

	HOMO-1	HOMO	LUMO	LUMO+1
HCQM1	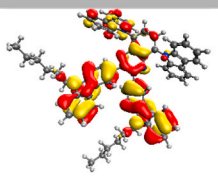 -5.22 eV	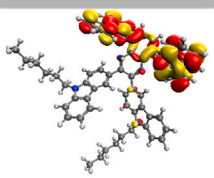 -5.15 eV	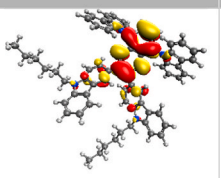 -2.06 eV	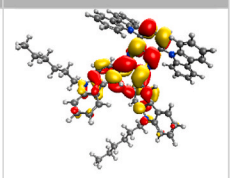 -1.19 eV
HCQM2	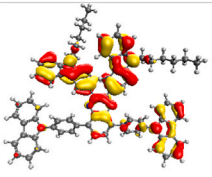 -5.24 eV	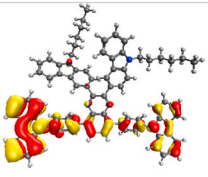 -5.18 eV	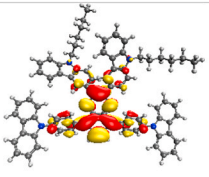 -1.97 eV	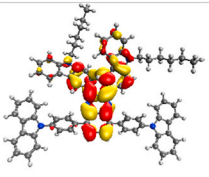 -1.11 eV

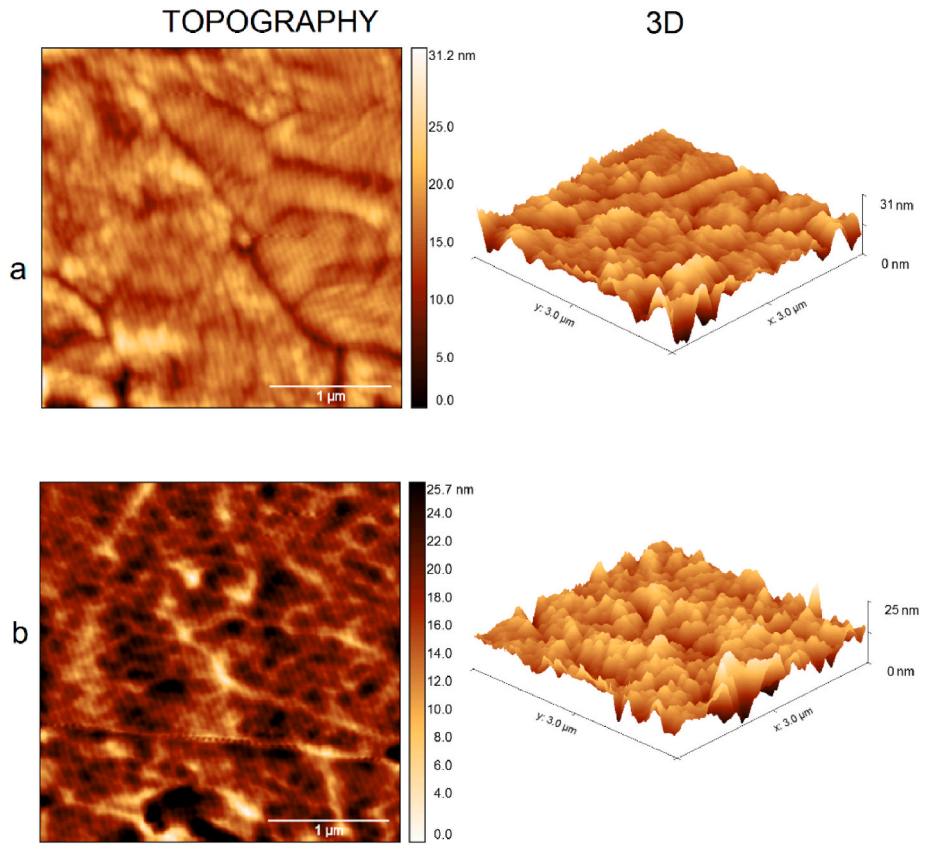

Fig. 6. AFM images of (a) poly(HCQM1) and (b) poly(HCQM2).

(HCQM2) films showed a single band between 375 and 550 nm in the neutral state, corresponding to the yellow color of the film (Fig. 7). This band was intensified in both polymer films, and a new absorption band centered at about 700 nm was attributed to polaronic and bipolaronic species formed along the polymer chain. Both poly(HCQM1) and poly (HCQM2) polymer structures are highly cross-linked because they polymerize over four carbazole units. As it is well known, during the electrochromic response, electrolyte ions provide color change as enter and exit into the polymer unit [51]. This could be owing to the more porous film surface of poly(HCQM2) observed from the AFM allowing the electrolyte to be easily injected and ejected from the polymer structure. Because of this reason, the increase in absorption band intensity and also optical contrast at poly(HCQM2) was found to be higher than that of poly(HCQM1). Finally, the yellow color of the poly (HCQM2) film turned into green and dark blue when applied the positive potential between 0 and 1.3V. On the other hand, the yellow color of the poly(HCQM1) film could only change to dark green between 0 and 1.35V. The observed color code according to International Commission on Illumination/Commission (CIE) was shown in Table 4.

The chronoamperometry technique was used to determine the electrochromic properties of poly(HCQM1) and poly(HCQM2), such as response time, optical contrast (ΔT%), and stability against applied potential changes (Fig. 8). By switching between the redox potential steps with a residence time of 10s, the changes in transmittance of the polymer films were investigated. The first and last 10 scans were also shown in Fig. S10. According to the results, the poly(HCQM1) film retained 71% of its optical activity after 1000 scans. On the other hand, it was observed that poly(HCQM2) was 15% more stable after 1000 scans compared to poly(HCQM1). The high stability of poly(HCQM2) is also consistent with AFM results, which are directly related to the

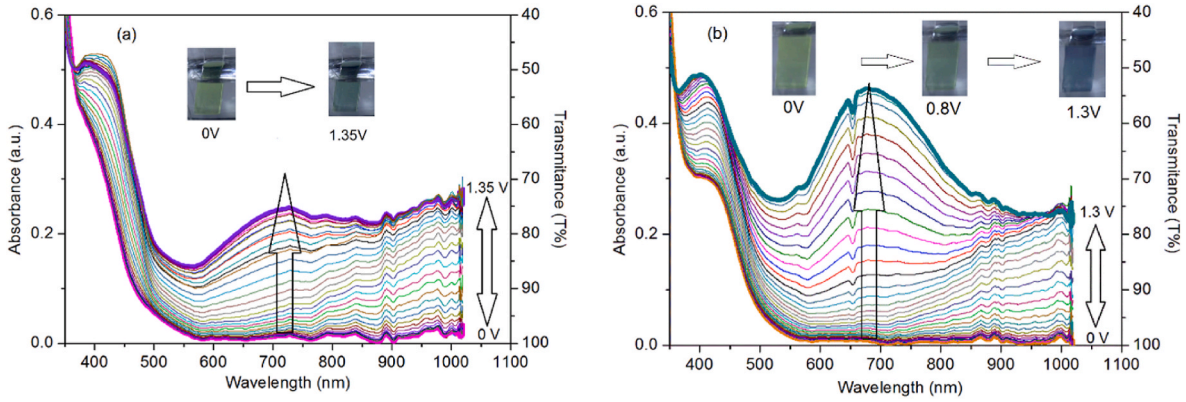

Fig. 7. Spectroelectrochemical measurements of poly(HCQM1) (a) and poly(HCQM2) (b) films deposited on ITO/glass surface with applied potentials.

Table 4
Electrochromic parameters of poly(HCQM1) and poly(HCQM2) films at 690 nm.

Polymer	Color code (L, a, b)	Optical contrast at (ΔT%)	Response Time (s)	Optical activity after 1000 cycles (%)	Coloration efficiency (cm^2/C)
poly(HCQM1)	*Neutral (0V)* L: 44.4, a: −10.6, b: 7.4 *Oxidized (1.35V)* L: 36.8, a: −8.4, b: −5.2	ΔT: 25% $T_{neut.}$: 96% $T_{oxi.}$: 71%	Oxidation 4.3 s Reduction 2.9 s	71%	85
poly(HCQM2)	*Neutral (0V)* L: 51.5, a: −11.4, b: 8.9 *Oxidized-1 (0.8V)* L: 42.7, a: −8.2, b: −2.3 *Oxidized-2 (1.30V)* L: 33.7, a: −3.1, b: −17.9	ΔT: 48% $T_{neut.}$: 96% $T_{oxi.}$: 48%	Oxidation 2.4 s Reduction 1.1 s	84%	268

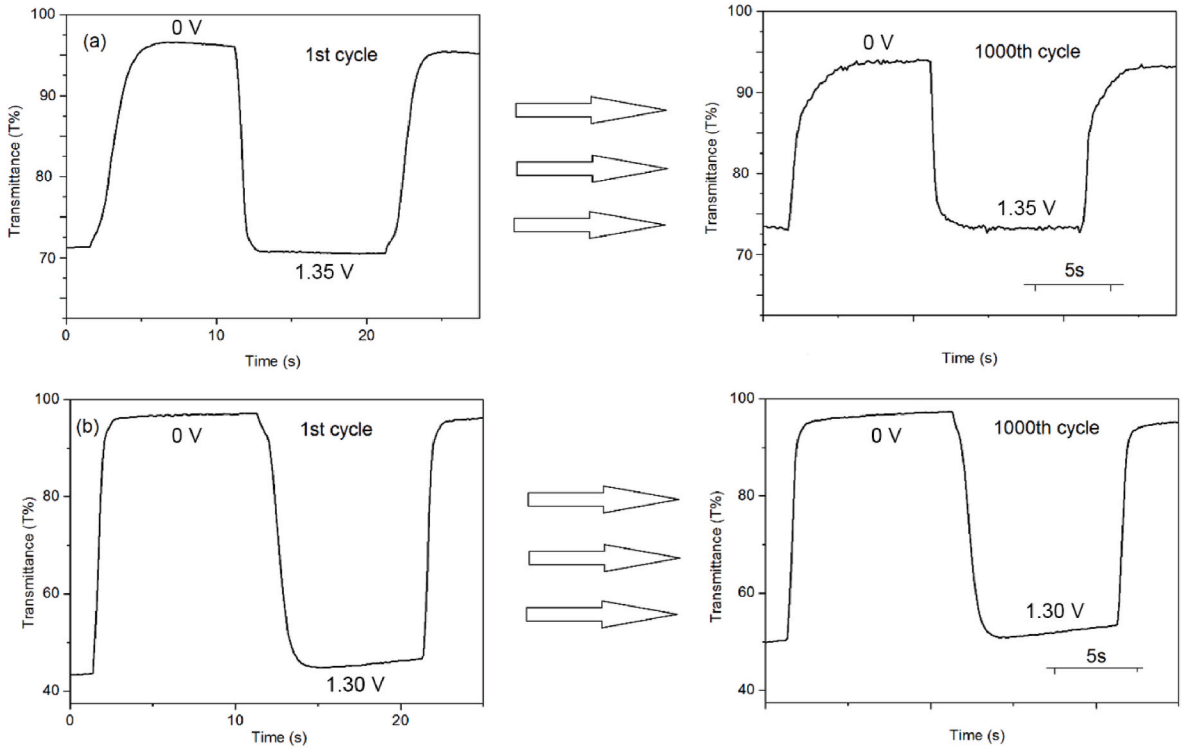

Fig. 8. Electrochromic switching and optical absorbance were monitored at 690 nm for poly(HCQM1) and poly(HCQM2).

morphology of polymer films [52,53]. Because of the similar effect, the oxidation/reduction response time of poly(HCQM2) was found to be significantly faster than that of poly(HCQM2) (HCQM1). Finally, the coloration efficiency values of poly(HCQM1) and poly(HCQM2) were calculated as 85 cm^2 C^{-1} and 268 cm^2 C^{-1}, respectively, using the equations of CE = ΔOD/Q_d, where Q_d: the injected/ejected charges between the redox states (Table 4). When compared to poly(HCQM2) with similar electroactive moieties, the coloration efficiency value of poly(HCQM1) was increased approximately three times by adding only the phenyl ring to the structure between the carbazole/donor and quinoxaline/acceptor units. When the obtained results are compared with the literature, it is seen that these values are quite good. The reason for this is thought to improve the coloration efficiency with the addition of an extra chromophore donor-carbazole group added to the structure [54,55].

4. Conclusion

Herein, the effect of phenyl spacer unit carbazole-based electroactive spaced containing quinoxaline as acceptor unit on their electrochemical optical and electrochromic properties was investigated. When compared to HCQM1, HCQM2 with a phenyl spacer moiety between carbazole/donor and quinoxaline/acceptor caused a blue shift in the optical absorption band with the lowest energy and slightly increased the oxidation potential at CV measurement. Theoretical DFT results are also consistent with optical and electrochemical data. AFM measurements revealed that poly(HCQM2) had a rougher thin film surface than poly (HCQM1) obtained from the potentiodynamic electrochemical polymerization process. Finally, it has been realized that the electrochromic performance of poly(HCQM2) is significantly better than that of poly (HCQM1) because of more interaction of electrolyte ions with the rough thin film surface of poly(HCQM2) (HCQM2). Furthermore, the electroactive molecules poly(HCQM1) and poly(HCQM2) synthesized are considered candidate materials for OLEDs and perovskite solar cells used in the emissive layer or hole transport layer, respectively.

CRediT authorship contribution statement

Ceylan Doyranlı: Investigation, Methodology. **Sinem Altınısık:** Investigation, Data curation. **Mücahit Özdemir:** Investigation, Software. **Sermet Koyuncu:** Writing – original draft, Writing – review & editing, Supervision.

Declaration of competing interest

The authors declare that they have no known competing financial interests or personal relationships that could have appeared to influence the work reported in this paper.

Acknowledgement

The numerical calculations reported in this paper were fully performed at TUBITAK ULAKBIM, High Performance and Grid Computing Center (TRUBA resources).

Appendix A. Supplementary data

Supplementary data to this article can be found online at https://doi.org/10.1016/j.dyepig.2022.110467.

References

[1] Mortimer RJ. Electrochromic materials. Chem Soc Rev 1997;26(3):147–56.
[2] Madasamy K, Velayutham D, Suryanarayanan V, Kathiresan M, Ho K-C. Viologen-based electrochromic materials and devices. J Mater Chem C 2019;7(16):4622–37.
[3] Cai G, Wang J, Lee PS. Next-generation multifunctional electrochromic devices. Acc Chem Res 2016;49(8):1469–76.
[4] Wang Z, Wang X, Cong S, Geng F, Zhao Z. Fusing electrochromic technology with other advanced technologies: a new roadmap for future development. Mater Sci Eng R Rep 2020;140:100524.
[5] Yun TG, Park M, Kim D-H, Kim D, Cheong JY, Bae JG, et al. All-transparent stretchable electrochromic supercapacitor wearable patch device. ACS Nano 2019;13(3):3141–50.
[6] Yang P, Sun P, Mai W. Res. Mater. Today. 2016;19(7):394–402.
[7] Moon HC, Lodge TP, Frisbie CD. Solution processable, electrochromic ion gels for sub-1 V, flexible displays on plastic. Chem Mater 2015;27(4):1420–5.
[8] Yan C, Kang W, Wang J, Cui M, Wang X, Foo CY, et al. Stretchable and wearable electrochromic devices. ACS Nano 2014;8(1):316–22.
[9] Kim YM, Moon HC. Ionoskins: nonvolatile, highly transparent, ultrastretchable ionic sensory platforms for wearable electronics. Adv Funct Mater 2020;30(4):1907290.
[10] Sella C, Maaza M, Nemraoui O, Lafait J, Renard N, Sampeur Y. Preparation, characterization and properties of sputtered electrochromic and thermochromic devices. Surf Coating Technol 1998;98(1):1477–82.
[11] Tian Y, Zhang X, Dou S, Zhang L, Zhang H, Lv H, et al. A comprehensive study of electrochromic device with variable infrared emissivity based on polyaniline conducting polymer. Sol Energy Mater Sol Cell 2017;170:120–6.
[12] Laschuk NO, Ebralidze II, Easton EB, Zenkina OV. Systematic design of electrochromic energy storage devices based on metal–organic monolayers. ACS Appl Energy Mater 2021;4(4):3469–79.
[13] Wang K, Wu H, Meng Y, Zhang Y, Wei Z. Integrated energy storage and electrochromic function in one flexible device: an energy storage smart window. Energy Environ Sci 2012;5(8):8384–9.
[14] Zhong Y, Xia X, Mai W, Tu J, Fan HJ. Integration of energy harvesting and electrochemical storage devices. 2017;2(12):1700182.
[15] Kim J, Rémond M, Kim D, Jang H, Kim E. Electrochromic conjugated polymers for multifunctional smart windows with integrative functionalities. 2020;5(6):1900890.
[16] Ansari SP, Ali F. Conjugated organic polymers for optoelectronic devices. In: Jafar Mazumder MA, Sheardown H, Al-Ahmed A, editors. Functional polymers. Cham: Springer International Publishing; 2018. p. 1–40.
[17] Durmus A, Gunbas GE, Camurlu P, Toppare L. A neutral state green polymer with a superior transmissive light blue oxidized state. Chem Commun 2007;(31):3246–8.
[18] Sonmez G. Polymeric electrochromics. Chem Commun 2005;(42):5251–9.
[19] Beverina L, Pagani GA, Sassi M. Multichromophoric electrochromic polymers: colour tuning of conjugated polymers through the side chain functionalization approach. Chem Commun 2014;50(41):5413–30.
[20] Gunbas GE, Camurlu P, Akhmedov IM, Tanyeli C, Onal AM, Toppare L. A fast switching, low band gap, p- and n-dopable, donor-acceptor type polymer. J Electroanal Chem 2008;615(1):75–83.
[21] van Mullekom HAM, Vekemans JAJM, Havinga EE, Meijer EW. Developments in the chemistry and band gap engineering of donor–acceptor substituted conjugated polymers. Mater Sci Eng R Rep 2001;32(1):1–40.
[22] Koyuncu S, Kaya İ, Koyuncu FB, Ozdemir E. Electrochemical, optical and electrochromic properties of imine polymers containing thiophene and carbazole units. Synth Met 2009;159(11):1034–42.
[23] Niu H, Kang H, Cai J, Wang C, Bai X, Wang W. Novel soluble polyazomethines with pendant carbazole and triphenylamine derivatives: preparation, characterization, and optical, electrochemical and electrochromic properties. Polym Chem 2011;2(12):2804–17.
[24] Kala K, Manoj N. A carbazole based "Turn on" fluorescent sensor for selective detection of Hg2+ in an aqueous medium. RSC Adv 2016;6(27):22615–9.
[25] Zou Q, Tao F, Wu H, Yu WW, Li T, Cui Y. A new carbazole-based colorimetric and fluorescent sensor with aggregation induced emission for detection of cyanide anion. Dyes Pigments 2019;164:165–73.
[26] Mirle CR, Raja M, Vasudevarao P, Sankararaman S, Kothandaraman R. Functionalised carbazole as a cathode for high voltage non-aqueous organic redox flow batteries. New J Chem 2020;44(34):14401–10.
[27] Yao M, Senoh H, Sakai T, Kiyobayashi T. Redox active poly(N-vinylcarbazole) for use in rechargeable lithium batteries. J Power Sources 2012;202:364–8.
[28] Sotzing GA, Reddinger JL, Katritzky AR, Soloducho J, Musgrave R, Reynolds JR, et al. Multiply colored electrochromic carbazole-based polymers. Chem Mater 1997;9(7):1578–87.
[29] Xu J, Ji Q, Kong L, Du H, Ju X, Zhao J. Soluble electrochromic polymers incorporating benzoselenadiazole and electron donor units (carbazole or fluorene): synthesis and electronic-optical properties. Polymers 2018;10(4).
[30] Contal E, Sougueh CM, Lakard S, Et Taouil A, Magnenet C, Lakard B. Investigation of polycarbazoles thin films prepared by electrochemical oxidation of synthesized carbazole derivatives. 2019;6(131).
[31] Lee JY, Han S-Y, Lim B, Nah Y-C. A novel quinoxaline-based donor-acceptor type electrochromic polymer. J Ind Eng Chem 2019;70:380–4.
[32] Yue H, Guo X, Du Y, Zhang Y, Du H, Zhao J, et al. Synthesis and characterization of donor–acceptor type quinoxaline-based polymers and the corresponding electrochromic devices with satisfactory open circuit memory. Synth Met 2021;271:116619.
[33] Karabiyik E, Sefer E, Baycan Koyuncu F, Tonga M, Özdemir E, Koyuncu S. Toward purple-to-green-to-transmissive-to-black color switching in polymeric electrochrome. Macromolecules 2014;47(24):8578–84.
[34] Pıravadılı S, Doyranlı C, Altınısık S, Bilgili H, Canımkurbey B, Koyuncu S. Fluorene-based donor-acceptor-type multifunctional polymer with bicarbazole pendant moiety for optoelectronic applications. J Polym Sci 2021;59(16):1829–40.
[35] Rybakiewicz R, Ganczarczyk R, Charyton M, Skorka L, Ledwon P, Nowakowski R, et al. Low band gap donor-acceptor-donor compounds containing carbazole and naphthalene diimide units: synthesis, electropolymerization and spectroelectrochemical behaviour. Electrochim Acta 2020;358:136922.
[36] Lifshits LM, Budkina DS, Singh V, Matveev SM, Tarnovsky AN, Klosterman JK. Solution-state photophysics of N-carbazolyl benzoate esters: dual emission and order of states in twisted push–pull chromophores. Phys Chem Chem Phys 2016;18(39):27671–83.
[37] Ning Z, Tian H. Triarylamine: a promising core unit for efficient photovoltaic materials. Chem Commun 2009;(37):5483–95.
[38] Heinze J, Frontana-Uribe BA, Ludwigs S. Electrochemistry of conducting polymers—persistent models and new concepts. Chem Rev 2010;110(8):4724–71.
[39] Patil AO, Heeger AJ, Wudl F. Optical properties of conducting polymers. Chem Rev 1988;88(1):183–200.
[40] Kaim W, Fiedler J. Spectroelectrochemistry: the best of two worlds. Chem Soc Rev 2009;38(12):3373–82.
[41] Ambrose JF, Nelson RF. Anodic oxidation pathways of carbazoles: I. carbazole and N-substituted derivatives. J Electrochem Soc 1968;115(11):1159.
[42] Karon K, Lapkowski M. Carbazole electrochemistry: a short review. J Solid State Electrochem 2015;19(9):2601–10.
[43] Frisch M, Trucks G, Schlegel H, Scuseria G, Robb M, Cheeseman J, et al. Gaussian 16. Wallingford, CT: Gaussian, Inc.; 2016.
[44] Dennington R, Keith TA, Millam JM. GaussView. Shawnee Mission, KS, USA: Semichem Inc.; 2009. Version 6.
[45] Becke AD. Density-functional exchange-energy approximation with correct asymptotic behavior. Phys Rev 1988;38(6):3098.
[46] Becke AD. Becke's three parameter hybrid method using the LYP correlation functional. J Chem Phys 1993;98:5648–52.
[47] Lee C, Yang W, Parr RG. Development of the Colle-Salvetti correlation-energy formula into a functional of the electron density. Phys Rev B 1988;37(2):785.
[48] Tomasi J, Mennucci B, Cancès E. The IEF version of the PCM solvation method: an overview of a new method addressed to study molecular solutes at the QM ab initio level. J Mol Struct: THEOCHEM 1999;464(1–3):211–26.
[49] Tomasi J, Mennucci B, Cammi R. Quantum mechanical continuum solvation models. Chem Rev 2005;105(8):2999–3094.
[50] Lee WJ, Fang YK, Ho J-J, Hsieh WT, Ting SF, Huang D, et al. Effects of surface porosity on tungsten trioxide(WO3) films' electrochromic performance. J Electron Mater 2000;29(2):183–7.
[51] Pan B-C, Chen W-H, Hsiao S-H, Liou G-S. A facile approach to prepare porous polyamide films with enhanced electrochromic performance. Nanoscale 2018;10(35):16613–20.
[52] Poverenov E, Li M, Bitler A, Bendikov M. Major effect of electropolymerization solvent on morphology and electrochromic properties of PEDOT films. Chem Mater 2010;22(13):4019–25.
[53] Zhang W, Wang X, Wang S, Zhu S, Wang Q. Morphology and electrochromic properties of nanostructured polyterthiophene films formed by different deposition modes. Sol Energy Mater Sol Cell 2021;230:111269.
[54] Lim B, Han S-Y, Jung S-H, Jung YJ, Park JM, Lee W, et al. Synthesis and electrochromic properties of a carbazole and diketopyrrolopyrrole-based small molecule semiconductor. J Ind Eng Chem 2019;80:93–7.
[55] Zhang Y, Kong L, Ju X, Du H, Zhao J, Xie Y. Synthesis and characterization of novel donor–acceptor type neutral green electrochromic polymers containing an indolo [3, 2-b] carbazole donor and diketopyrrolopyrrole acceptor. RSC Adv 2018;8(38):21252–64.